Materiales de Construcción
Vol. 71, Issue 344, October-December 2021, e262
ISSN-L: 0465-2746
https://doi.org/10.3989/mc.2021.11021

Characterisation and diagnosis of heritage concrete: case studies at the Eduardo Torroja Institute, Madrid, Spain

P.M. Carmona-Quiroga[a] ✉, A. Pachón-Montaño[a], J. Queipo-de-Llano[a], J.A. Martín-Caro[b,c], D. López[b], I. Paniagua[b], I. Martínez[a], F. Rubiano[a], I. García-Lodeiro[a], L. Fernández-Ordóñez[d], M.T. Blanco-Varela[a], E. Frías-López[a]

a Eduardo Torroja Institute for Construction Science (IETcc, CSIC), (Madrid, Spain)
b. Ines Ingenieros Consultores, (Madrid, Spain)
c. ETSICCP, Universidad Politécnica de Madrid, (Madrid, Spain)
d. Estudio Guadiana, (Madrid, Spain)
✉: pcarmona@iqfr.csic.es

Received 15 July 2021
Accepted 29 September 2021
Available on line 11 November 2021

ABSTRACT: That the preservation of twentieth concrete heritage is an area scantly explored can be attributed to a lack of appreciation for such a young material. In most cases conservation is broached from a technical perspective with little regard for heritage value. Ongoing assessment of the condition of structures is the primary strategy to minimise such misguided action. This study involved characterising the condition of the concrete in a number of singular elements forming part of the Eduardo Torroja Institute for Construction Science headquarters at Madrid, Spain, a modernist compound listed by the city of Madrid as a protected asset. The in situ findings using non-destructive and laboratory techniques revealed the core concrete to be in good condition. The surface material, however, exhibits signs of durability issues calling for conservation treatments and techniques compatible with the preservation of the integrity and authenticity of this young heritage material.

KEYWORDS: Concrete heritage; Weathering; Physical properties; Behaviour of large ages; Modern movement.

Citation/Citar como: Carmona-Quiroga, P.M.; Pachón-Montaño, A.; Queipo-de-Llano, J.; Martín-Caro, J.A.; López, D.; Paniagua, I.; Martínez, I.; Rubiano, F.; García-Lodeiro, I.; Fernández-Ordóñez, L.; Blanco-Varela, M.T.; Frías-López, E. (2021) Characterisation and diagnosis of heritage concrete: case studies at the Eduardo Torroja Institute, Madrid, Spain. Mater. Construcc. 71 [344], e262. https://doi.org/10.3989/mc.2021.11021.

RESUMEN: *Caracterización y diagnóstico del hormigón patrimonial: Casos de estudio en el Instituto Eduardo Torroja, Madrid, España.* La conservación del patrimonio del siglo XX en hormigón apenas se ha explorado. Los escasos estudios de este tipo se abordan desde una perspectiva técnica sin tener en cuenta su valor patrimonial. La principal estrategia para minimizar su deterioro es la evaluación continua del estado de conservación de estos bienes. En este estudio se caracterizó estado del hormigón en una serie de elementos singulares que forman parte de la sede modernista del Instituto Eduardo Torroja de Ciencias de la Construcción en Madrid, España, catalogado por la ciudad de Madrid como un bien de interés cultural. Los resultados obtenidos in situ con técnicas no destructivas y los análisis de laboratorio revelaron que el interior de los hormigones se encuentra en buen estado. La superficie, en cambio, presenta problemas de durabilidad que requieren tratamientos de conservación y técnicas compatibles con la preservación de la integridad y autenticidad de este joven material patrimonial.

PALABRAS CLAVE: Patrimonio en hormigón; Deterioro; Propiedades físicas; Comportamiento a largas edades; Movimiento moderno.

1. INTRODUCTION

1.1. General

The built cultural heritage is generally agreed to constitute a material element whose historic, documentary and aesthetic information merits preservation for future generations. Concrete heritage is the latest to be added to the list of materials, although not without some controversy (1). Its maintenance and conservation are not priority issues (2), for, in the absence of acknowledgement and appreciation, it is not deemed a tourist attraction. Nonetheless, the cultural significance of a growing number of concrete buildings is prompting listings as heritage assets (3-5).

Although as a material concrete can be traced back to the Roman Empire, when lime- and pozzolan-based hydraulic cement (opus caementicium) was discovered (6), the standardised production of concrete and its use in new forms of construction are fruit of the intellectual progress attendant upon the industrial revolution. In 1824 Joseph Aspdin patented a process for making portland cement (PC), whilst François Coignet used precast structural concrete for the first time in 1852 and S.T. Fowler was granted the first-ever patent for reinforced concrete technology in a wall built in 1860 (7).

French architects Auguste and Gustave Perret were often contemporarily credited for pointing the way to the modern use of concrete (7). It was not until the twentieth century, however, that it came to be regarded as a 'noble' material, used by modernist, brutalist and expressionist architects (5, 8, 9) and sculptors (10). That drove the international preference for concrete as a material able to modernise construction art (11). It has since become the predominant construction material (3, 12).

Historically emblematic concrete structures and buildings have already begun or will with time begin to show signs of decay, however (13-15). Due to the fairly recent advent of this construction material, a full understanding of its long-term behaviour and durability is still in the making (3). It is often in need of repair (16), subject as it is to decay induced by a number of physical, chemical and biological agents, most commonly carried by water (13, 17, 18).

Intermediate relative humidity establishes the optimal circumstances for carbonating primarily the $Ca(OH)_2$ (due to its relatively high solubility), but also all the other less soluble cementitious phases (CSH, AFm, AFt) of concrete (19). In addition, the removal of alkalis (Na, K, Ca) in the leaching processes modifies the composition of the pore solution and the stability of the said cementitious phases (20). The concomitant decline in internal pH destroys the passivity that protects the reinforcement, which corrodes as a result. If reinforcement corrosion is severe, the oxides clustering around the rebar may prompt concrete cracking, hastening decay or even inducing collapse in extreme cases (21). In coastal areas or where de-icing salts are used, chloride-induced reinforcement corrosion may also pose problems.

On occasion, decay may be particularly accentuated in historic concrete manufactured with high water/cement ratios to enhance workability (1, 22) or potentially reactive (aggregate-alkali alkali-aggregate reaction; metallic sulphides) local aggregate (18) due to the absence of regulatory standards (4, 14) and the knowledge gaps prevailing around decay mechanisms at the time of construction.

Certainly, concrete deteriorates whether it has patrimonial value or not (overloads, cyclical loads, impacts, exposure to extreme temperatures, surface erosion or abrasion, volume changes due to temperature or relative humidity gradients, expansive reactions or exchange, leachate etc.), however, the techniques and materials used in its repair often cannot be the same.

Insufficient understanding of the cause of decay or of the heritage significance of buildings and structures may result in inappropriate repair to the detriment of the architectural, historical and cultural content of the respective monuments (3, 13). As a rule, the repair techniques applied, designed for modern concrete (23), are not always satisfactory for the historic material, either because they are ineffective or because they fail to honour the principles laid down in international treaties (ICOMOS Charter of Venice and 2003 Charter (1, 13, 24)). That lack of understanding of the efficacy and durability of repair treatments is one of the challenges posed by heritage concrete conservation (25) a field that has only recently begun to come into the spotlight in the wake of a growing appreciation for modern heritage structures (3, 12, 13, 26). Recent research focuses on the development of specific water-repellent treatments (such as sealers) (27, 28) and compatible patch repair mortars (12).

Another challenge outstanding solution is the heightening of citizen awareness of the twentieth century's built heritage, for given the 'youth' of the material involved, the historic-cultural value of that heritage is not fully acknowledged. Such low appreciation and care raise the risk of decay (4). Europe's H2020 project, InnovaConcrete (29) was created against that backdrop. One of the project's main pillars is the selection and analysis of the 100 most significant concrete structures built in the 28 EU countries (30) as outstanding examples of technical, social and aesthetic innovation in twentieth century architecture and engineering. All those cultural, historical, aesthetic, social and technological innovation values provide the significance for their identification as heritage.

Another essential pillar is the development of multi-purpose materials and specific techniques for

the conservation of the concrete heritage whose implementation and commercialisation will be validated in laboratories and in the field on seven concrete monuments or singular European heritage structures chosen in keeping with scientific and humanistic criteria.

One of the seven case studies selected, the Eduardo Torroja Institute for Construction Science headquarters at Madrid, Spain, representative of interdisciplinary cooperation among twentieth century architects, engineers and concrete researchers, was chosen for that reason and on the grounds of the prominence of its founder, engineer Eduardo Torroja (31). Protected by the city of Madrid for the singularity of its concrete structures, the building is also listed in the registry of the modern movement kept by the Iberian Docomomo Foundation (32) and bears the honorary plaque awarded by the Chartered Institution of Madrid Architects' Bronze Club.

1.2. Historic analysis of the building, an InnovaConcrete case study

Eduardo Torroja, who played a major role in the scientific, technical and aesthetic revolution that preceded the rapid development of reinforced and prestressed concrete in the first half of the twentieth century (31), headed a group of architects and civil engineers who founded what today goes by the name of Eduardo Torroja Institute for Construction Science. It was the first institution in Spain to foster progress in all areas of construction and its materials (33). Construction of the present headquarters in 1951-1953 (Figure 1a), with its many precast members and singularly shaped concrete elements, constituted a genuine workbench at a time when Pier Luigi Nervi was conducting similar experiments in Italy (34). The main building's sober and functional lines are based on a single precast 1.60 m tall module (35) comprising tiled flooring, window and roof gutter (Figure 1b, c and d). That sobriety and functionality contrast with other more unique constructional and structural systems, such as the multi-pitched roof over the coal deposit (Figure 1e), the retaining wall that encloses the complex while also serving as a lookout shaded by a unique pergola with rib-like supports (Figure 1f); the pergola in the car park consisting in 'sidewise-seven'-shaped beam-columns (hereafter, car park pergola) (Figure 1g); and the outdoor chapel (36), a later addition consisting in a likewise rib-like concrete shell (Figure 1h) (37).

The building is sited in an urban environment on the outskirts of the city, surrounded by woodland and, since the late nineteen seventies, by Madrid's inner ring road. The weather conditions to which it has primarily been exposed are listed in Table 1. Recent years have witnessed a substantial rise in temperatures, with less rain- and snowfall. Atmospher-

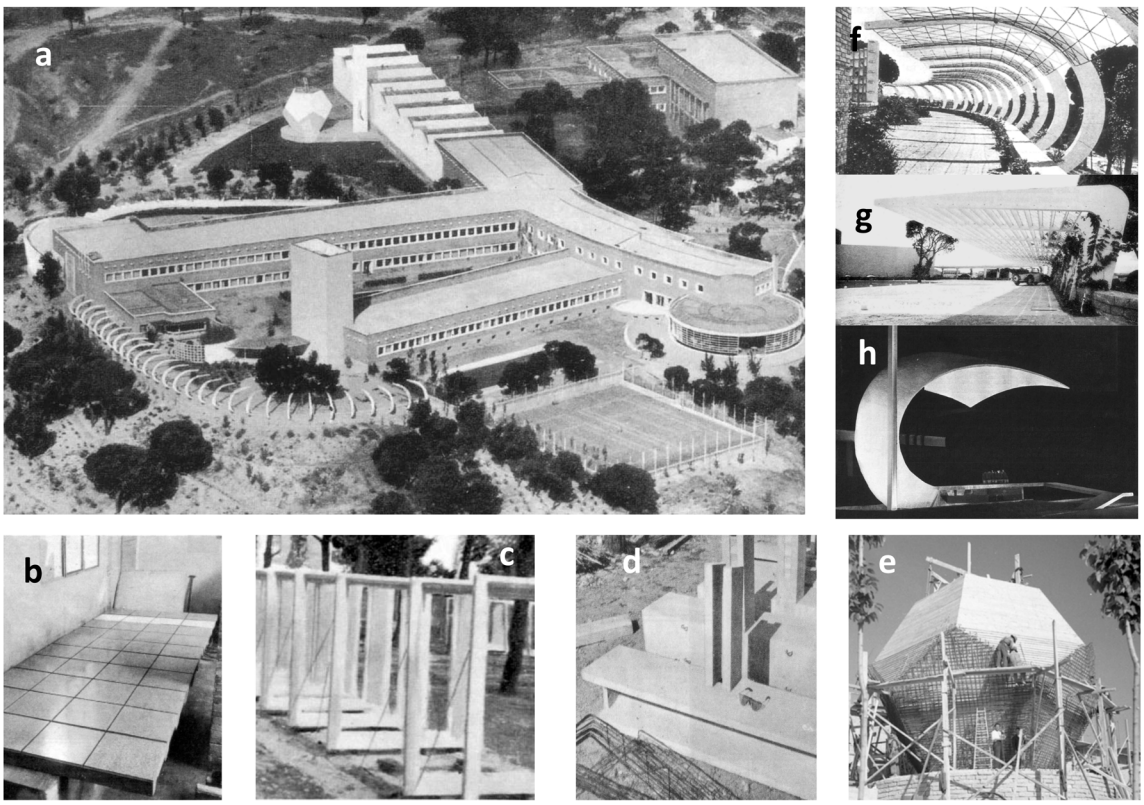

Figure 1. (a) Finished building (38). (b) Tile flooring (39). (c) Window frames (39). (d) Gargoyle (39). (e) Dodecahedral coal deposit (40). (f) Pergola with rib-like supports crowning enclosure wall (38). (g) Car park pergola (38). (h) Rib-like shell/outdoor chapel (37).

ic CO_2, source of concrete carbonation and loss of strength and durability when the material is not duly manufactured, has declined gradually since 2005 (16.18 kt CO_2 eq), with today's values (10.78 kt CO_2 eq, 2017) even lower than recorded in 1990.

Rain, occasional ice-thaw cycles and vehicle traffic- and heating-induced pollution are the most prominent agents of decay in the building's concrete structures, some of which were repaired before having rendered 70 years of service.

This study aimed to assess the present condition of the portland cement concrete (or mortar) structures in this singular building, a pre-requisite in historic construction revitalisation (4, 13). More specifically, it characterised the pathologies in three architectural elements that contribute to the building's unique identity: the window frames, the car park pergola and the rib-like concrete shell designed as an outdoor chapel. The necessarily cross-disciplinary approach (4, 24) adopted is based on historic and architectural records and the use of non-destructive techniques to collect geophysical data (4, 12, 14, 15). The structures chosen, representative of distinct stages in building construction (1953 and 1969), were built with different materials (concretes or mortars) and construction methods (precast or cast-in-place) and some but not all had been rehabilitated or maintained prior to the study.

Another purpose of diagnosis is to minimise the maintenance required via periodic inspection of structures and establish conservation strategies that preserve the original conditions as closely as possible. The measures envisaged include validation of innovative preventive treatments compatible with and optimised or developed under the InnovaConcrete project, including consolidants, water-repellents, corrosion inhibitors and micromortars.

In a broader scope, this investigation aims to contribute to the conservation of concrete of the 20th with cultural significance by characterising its pathologies from a preventive conservation perspective and by addressing, where appropriate, preventive conservation solutions (mainly novel protective treatments) which are compatible with established conservation principles in this case of study.

2. METHODOLOGY

The diagnostic campaign began with the study of all the information compiled on the building's constructional history, including original design drawings and specifications, historic documents on construction methods, materials used, earlier conservation operations and scientific papers.

The working plan drawn up after the aforementioned review and a preliminary visual inspection of the pathologies consisted in characterising the condition of the materials with laboratory physical-chemical tests and field measurements.

2.1 Laboratory characterisation of the concrete

Representative core samples were drawn from the elements studied for subsequent laboratory characterisation from low and relatively hidden areas apart from the window frame, where the sample taken was almost dislodged. The fine and coarse aggregates were examined under a Nikon Eclipse E600 optical microscope to determine their composition. The former was also studied with a field emission scanning electron microscope (FESEM) fitted with a Bruker 20-kV XFlash Detector 5030 energy dispersive X-ray spectrometer (EDX). Fines size was recorded as measured with the optical microscope and the medium-sized and large materials as determined with Image J software based on photographs taken

Table 1. Conditions prevailing in 2019 compared to a 30-year reference period (1981-2010): temperature and relative humidity recorded at a city meteo station a few km apart of the site of study and pollutant values.

Weather conditions (41, 42)	
High temperature, July (°C)	39.5 (1981-2010); 40.7 (2019)
Low temperature, January (°C)	−7.4 (1981-2010); −1.8 (2019)
Yearly mean temperature, July (°C)	25.6 (1981-2010); 28.0 (2019)
Yearly mean temperature, January (°C)	6.3 (1991-2010); 6.5 (2019)
Mean yearly rainfall (mm)	421.0 (1981-2010); 372.9 (2019)
Mean yearly number of frost days	15.7 (1981-2010)
Mean yearly number of snow days	3.6 (1981-2010)
Mean relative humidity (%)	57.0 (1981-2010)
Acid rain / other pollutants (42, 43)	
Mean yearly NO_2 (μg/m^3)	31 (mean); 220 (max.) (2019)
Yearly SO_2 (μg/m^3)	9 (mean); 53 (max.) (2019)
Yearly kt CO_2 eq	12.95 (1990); 16.18 (2005); 10.78 (2017)

with a standard camera or Kappa software based on binocular microscopic images. Aggregate sizes are given further to the d/D nomenclature defined in European standard BS EN 12620:2003+A1:2009 (44).

A fraction with high cement paste content was obtained from the core samples by mechanically separating as much of the sand and gravel as possible.

The resulting powder was then XRD-scanned with a Bruker D8 Advance 2.2-kW diffractometer (CuK-α1 radiation: 1.5406 Å; CuK-α2 radiation: 1.5444 Å) to identify the hydrated cement phases and detect the possible presence of altered products. KBr pellets bearing concrete or mortar samples were studied with a Nicolet 7600 FT-IR spectrometer (range, 4000–400 cm^{-1}; 32 scans; spectral resolution, 4 cm^{-1}) to determine their mineralogical composition. Their portlandite and calcite contents were quantified in platinum crucibles in a N_2 atmosphere at 1000 °C and a flow rate of 10 °C/min on a TA SDT Q600 TGC/DSA analyser.

Carbonation depth was determined by measuring the width of the unstained rim of fresh fractured surfaces sprayed with thymolphthalein (45) and sample homogeneity was assessed with a Pundit7 ultrasonic tester by determining the ultrasonic pulse velocity and respective longitudinal modulus of elasticity (MOEus) or Young's modulus.

Standard dissolution procedures (46) were used where appropriate to determine the cement:aggregate ratio.

Concrete density and water-accessible porosity were determined as set out in Spanish standard UNE 83980 (47).

The porosity of the window frame mortar was determined with a Micromeritics Autopore IV 9500 V1.05 Hg intrusion porosimeter. Cylindrical specimens measuring 40 mm in diameter and approximately 80 mm high were analysed for compressive strength on an Ibertest Autotest 200/10 test frame as specified in BS EN 12390-3:2020 (48).

Dry and saturated core sample electrical resistivity were measured using the direct electrochemical impedance spectroscopic (EIS) method (two external electrodes) (49). Readings were recorded on the FRA module of an Autolab 302 potentiostat/galvanostat operating at frequencies of 1 Hz to 1 MHz in potentiostatic mode with a sine wave amplitude of 350 V. Resistivity was calculated from the impedance module value at which an imaginary component was near zero. Concrete core specimens measured 40 mm in diameter and 49 mm and 43 mm high, respectively for the car park pergola and for rib-like shell structures.

2.2. In situ non-destructive testing

The field measurements consisted, firstly, in assessing possible structural anomalies by comparing the original design drawings for the car park pergola to the element as it presently stands. That assessment was informed by the topographic survey data generated by a FARO Technologies Focus 3D laser scanner (visual field, 305° vertical, 360° horizontal; range, 0.6 m to 120 m; resolution, 70 pixels) and converted to three dimensional lattices with FARO Scene 7.1 and Rhinoceros software. The 3D survey data for the rib-like shell were published in a paper by Echevarría et al. (50), whilst none was deemed necessary for the windows, in light of their straightforward geometry.

Reinforcement bar position and the thickness of the concrete cover were determined with a Hilti PS 1000 X-scan ground penetrating radar (GPR).

In-situ tests were likewise conducted to determine the condition of the concrete elements. Their surface hardness was measured with a Proceq DigiSchmidt Schmidt hammer (51) and the respective compressive strength values were calculated from the manufacturer's calibration curves.

Corrosion of the steel embedded in the concrete was assessed quanti- and qualitatively. The electrochemical parameters recorded for that purpose, all of which called for a ground connection to the steel, included: i) corrosion potential (E_{corr}) (52); ii) corrosion rate (I_{corr}) (modulated confinement method (53, 54); and iii) concrete resistivity (ρ) (galvanostatic pulse method (55)). All measurements were logged with a NAV-ECM corrosion rate meter.

Because water drives corrosion, the relative moisture in the elements was characterised. Up to 10 readings were taken with a DCL Metrología laser moisture meter in each area selected for analysis.

3. RESULTS AND DISCUSSION

3.1. Car park pergola

3.1.1. Historical background and present condition

Located in the car park, this outdoor structure comprises 22 'sidewise-seven'-like 2.5x5.55x0.17 m (height x length x thickness) supports spanned by wooden shading slats. Both concrete and slats (the latter not conserved) were initially painted white (Figure 2). The structural review was based on the original drawings and information in the general design specifications on the type of concrete and reinforcement used to build the supports (Table 2).

Surface spalling on the concrete members was patch-repaired in 2007 when the white paint, biological colonies, rust from the exposed reinforcement and poorly bonded grout were sand-blasted off the supports. An epoxy resin passive seal (Legaran by Degussa) was subsequently applied to protect the exposed steel rebar and ensure the bond (with hydraulic binders and resins (Degussa PCC-20)) to the patch mortar used to restore the detached cover.

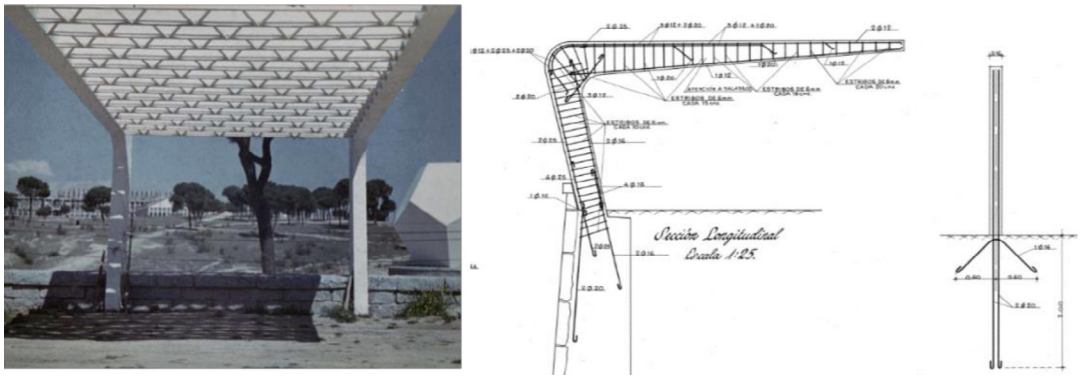

FIGURE 2. Car park pergola: construction and reinforcement drawings (38).

TABLE 2. Key characteristics of pergola concrete.

	Design specifications (40, 57, 58)	**Findings in this study**	**Eurocode** (56)
Compressive strength (MPa)	17.16	30	30
Water-accessible porosity (v/v %)	≤5 % to 6 % (concrete wt)	9.8	7 – 24
Density (g/cm³)		2.3	2.4 - 2.9
Cement content (kg/m³)	300-350		>300
Type of cement	Portland or alumina	Grey portland	
Gravel aggregate	800 L/m³ to 900 L/m³ natural or crushed aggregate	Natural aggregate: carbonates, quartz polycrystalline	
Sand aggregate	400 L/m³ to 500 L/m³ siliceous sand	siliceous sand: quartz, potassium feldspar, plagioclase, schist	
Moisture (%)		30.01 % to 43.6 %	
Ultrasound velocity (m/s)		4471	
Young's mod. (GPa)		41.4	
Dry resistivity (kΩ·cm)		145.38	
Saturated resistivity (kΩ·cm)		8.45	
Reinforcement bar cover (mm)	> 30	0-30 (mostly 10-25)	35
Carbonation depth (mm)		9 ± 3	

All the surfaces were then painted with Masterseal 325E, a white anti-carbonation coating to detain reinforcement corrosion.

The present visual inspection (Figure 3) revealed concrete cracking at the top and especially at the tip (Figure 3(b)) of the supports, material loss, biological colonisation and corrosion in the exposed rebar.

3.1.2. Concrete characterisation

The pergola concrete was characterised to identify the possible origin of the damage and any necessary repairs to choose compatible materials or treatments.

The most prominent physical properties defined in the original design (40, 57) and the ones determined from the core samples in this study are given in Table 2, along with other provisions on concrete set out in the Eurocode (56) for new structures exposed to similar environmental conditions.

Aggregate size distribution was determined by analysing the macroscopic (with no or low enlargement) and (optical and electronic) microscopic images of the core samples (Figure 4), which also revealed their composition, found to be: in the gravel (d/D=2.5/28), carbonate (micritic texture) and polycrystalline quartz grains (with and without mica and iron oxides); in the sand (d/D=0.05/2.5), primarily monocrystalline quartz, and secondarily metamorphic rock fragments (schist), potassium feldspar (microcline) and plagioclase (albite). Both size and

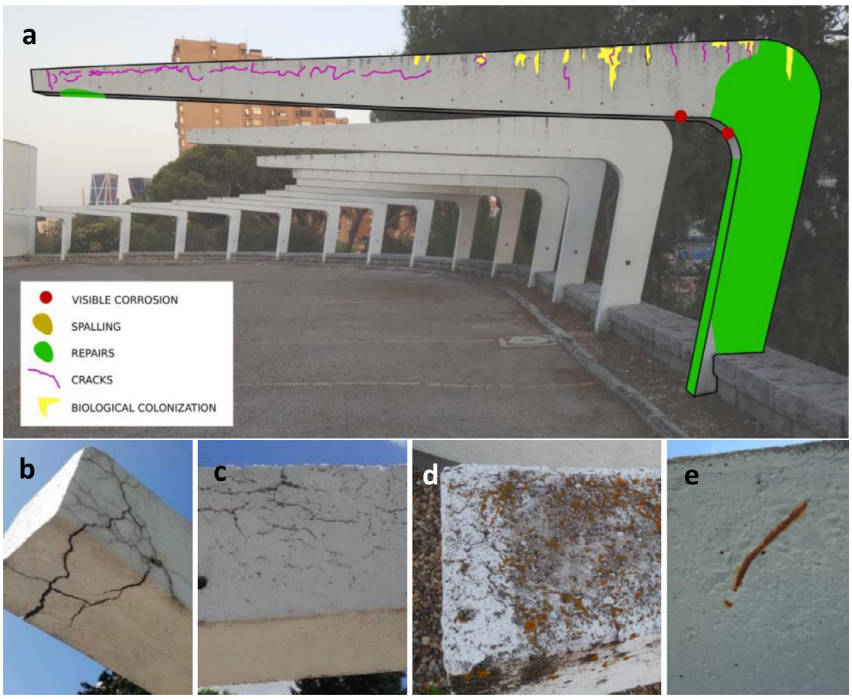

FIGURE 3. Damage mapping in the car park pergola: (a) Diagnosis. (b) Significant cracking. (c) profuse cracking. (d) Biological colonisation. (e) Steel corrosion.

composition were largely in agreement with the design specifications (57), which called for 800 L/m^3 to 900 L/m^3 of natural or crushed gravel with up to 3 % clay and 400 L/m^3 to 500 L/m^3 of rinsed siliceous sand with a maximum size of 38 mm and no more than 10 % clay of a maximum size of 5 mm (50 % coarse grain from 2 mm to 5 mm and up to 15 % medium grain, from 0.5 mm to 2 mm).

The mixed (siliceous and calcareous) composition of the aggregates ruled out the use of both the standard procedure for determining cement content (46) based on the HCl-solubility of silica at 5 °C and the calcium oxide sub-procedure. The design specified a cement content of 300 kg/m^3 to 350 kg/m^3.

The XRD pattern for the high cement content paste contained reflections for the two primary hydrated phases, ettringite and portlandite, along with signals for gypsum, perhaps attributable to the deposition of atmospheric SO_2 (59). The most intense lines identified the quartz, calcite, feldspars, albite and microcline present in the aggregates (Figure 5a). The signals for calcite might also have been generated as a result of cement paste carbonation. Further to the DTA/TG study, this hydrated cement-high sample contained 22 wt% calcite and 5 wt% portlandite, denoting the persistence of a store of alkalinity available for reinforcement passivation (60).

The FT-IR spectrum, in turn, exhibited the bands characteristic of the aforementioned mineral phases (Figure 5b): calcite at 1425, 875 and 712 cm^{-1}; silicate vibrations at around 1000 cm^{-1}; the double band characteristic of quartz at 796 cm^{-1} and 777 cm^{-1}; the bending vibrations typical of the S-O in sulfates at 668 cm^{-1}; and the stretching vibrations generated by the OH groups in portlandite at 3640 cm^{-1} (61).

The carbonation front in the sample core was not

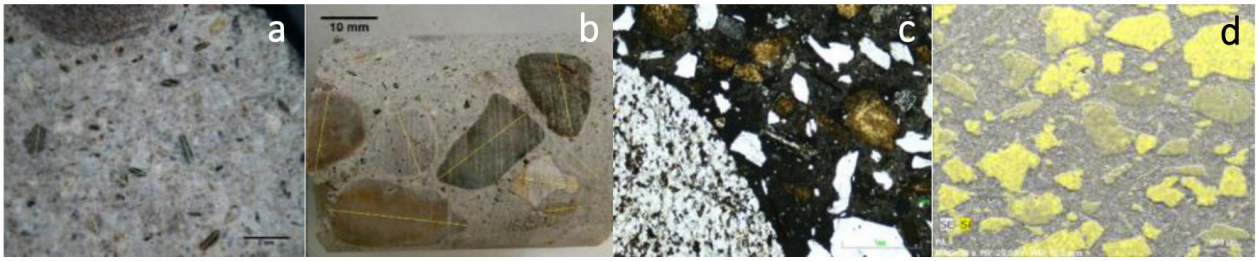

FIGURE 4. Photo- and micrographic scale images for determining aggregate particle size distribution in the pergola concrete: (a) Standard camera. (b) 2x binocular microscope. (c) polarized light microscope. (d) BSEM-EDX.

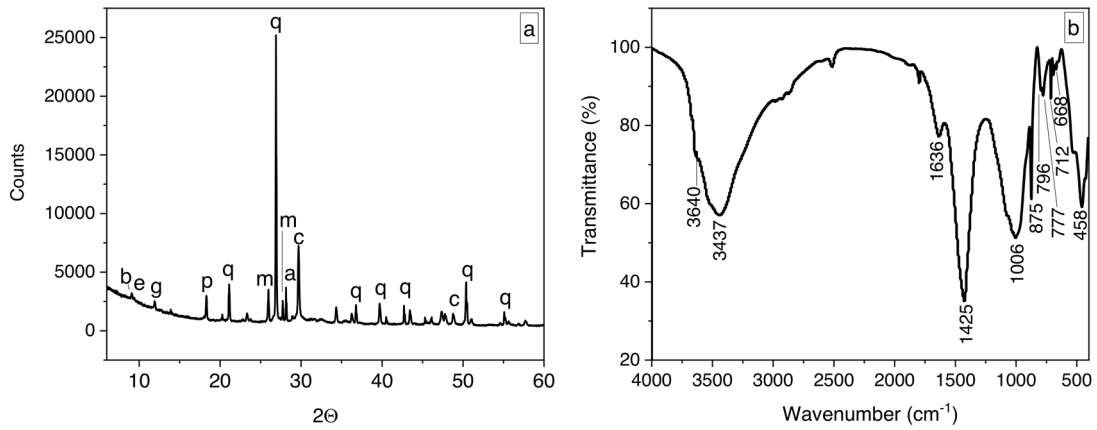

FIGURE 5. Pergola concrete components identified by: (a) XRD, where b=biotite (COD: 9000025) e=ettringite (COD: 9011103); g=gypsum (COD: 1010981); p=portlandite (COD: 9009098); m=microcline (COD: 9000189); q=quartz (COD: 1011159); a=albite (COD: 9001631); c=calcite (COD: 9007689). (b) FT-IR.

very deep, despite the high levels of air pollution to which the material has been exposed over the years: mean CO_2 penetration was 8.7 mm, with a maximum of 12 mm (Figure 6, Table 2).

The concrete's water-accessible porosity was a moderate 9.8 % (Table 2) while its density was 2.3 g/cm^3 which, like its Young's modulus, lay within the range defined in Eurocode BS EN 1992-1-1 (56) At 30 MPa its compressive strength, far higher than the design value, was likewise as recommended in (56) for concrete in standard structures.

Core specimen electrical resistivity, found (prior to mechanical characterisation) to assess the risk of steel corrosion, was 8.45 kΩ·cm under saturated and 145.48 kΩ·cm under dry conditions. Further to the criterion proposed by Polder et al. (53) for saturated conditions, here the reinforcement would be at high risk of corrosion, given its low resistivity, <10 kΩ·cm. The severity of that risk is relativised, however, by the structure's location in an area where neither humidity nor the presence of chlorides is high. For fuller information in that regard, in situ measurements were made of electrical resistivity, corrosion potential and corrosion rate (E_{corr}, mV; I_{corr}, μA/cm^2) (see item 3.1.3).

By way of summary, according to the laboratory tests conducted the concrete was in good condition further to its age and location.

3.1.3. In-situ testing

Laser scans were captured of the 22 units comprising the structure (Figure 7(a)) to compare their present 3D geometries to the original design drawings. The results for rib No. 8 reproduced in Figure 7(b) (ribs numbered consecutively beginning with the one closest to the building) showed that the built geometry was nearly identical to the design, with minor deviations possibly due to stake-out errors or to the time

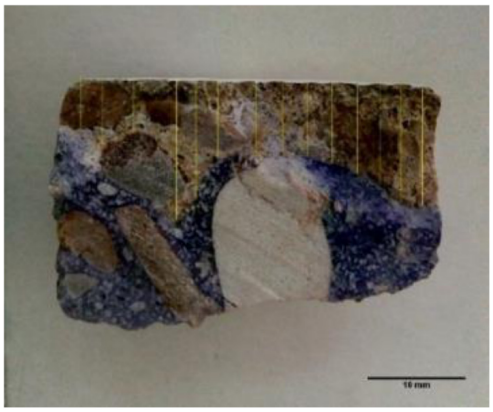

FIGURE 6. Surface of freshly broken core sample drawn from the car park pergola after spraying with thymolphthalein (blue dye = non-carbonated material).

lapsing since construction. The 8 cm to 15 cm slump at the edge of the overhang relative to the design and a curved deformation on its upper side together determined a 0.8 cm to 2 cm difference in mid-span height. Although the value of the slump appearing initially is unknown, the curved deformation along the top of the element might hold a clue to the deflection incurred since it was built (bearing in mind that the formwork used was flat). That relative deformation is in keeping with today's legislative provisions on the construction of cantilevered structural floors in buildings (62). The rest of the slump may be due to rotation in the restrained end, as the overlain geometries (Figure 7(b)) would appear to indicate, and/or related to flawed workmanship or levelling during construction. Moreover, the pergola has to bear only its own weight and no pathologies were observed that would entail structural risk. The deformation nonetheless generates

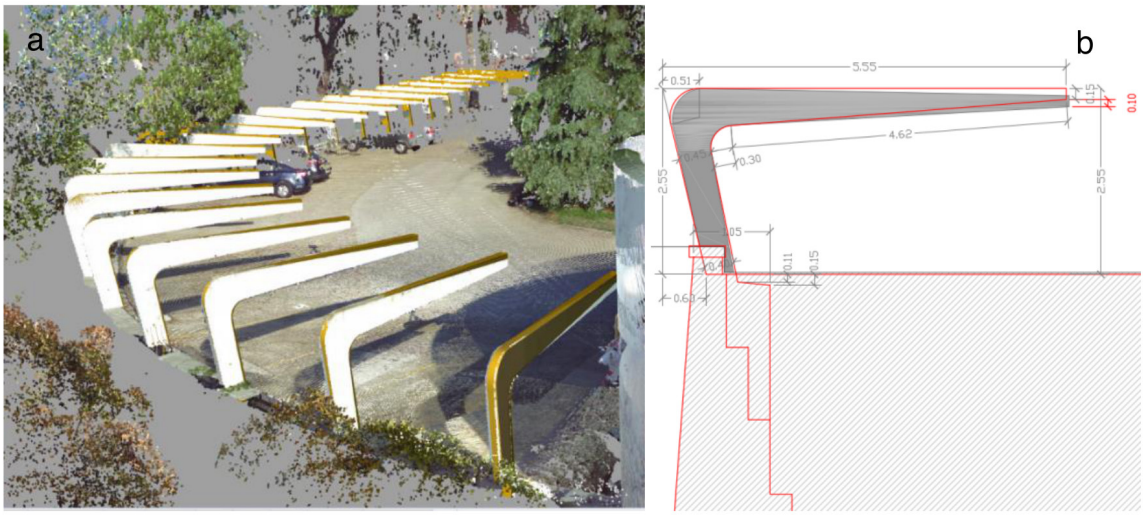

FIGURE 7. (a) Point cloud (white units) and design geometry (gold unit). (b) Design (red outlining, grey lettering) and built (grey shading) geometries and deformation (red lettering).

tensile stress in the top surface of the overhang that favours the appearance of small or the enlargement of existing cracks on that surface, the one most exposed to rainwater. It should consequently be protected to prevent subsequent pathologies.

The ground-penetrating radar (GPR) findings showed that the concrete cover, at <30 mm (Table 2), fails to meet both the design specifications, which call for a cover thickness of >30 mm, and the 35 mm minimum presently laid down in the Eurocode (56) for class 4 structures (buildings and other common structures) with XC4 exposure (outdoor structures).

The electrical resistivity and corrosion potential measurements were below the threshold values defined for steel de-passivation, indicating negligible corrosion and high levels of steel corrosion resistance at this time (Figure 8). All the corrosion rate readings taken in the on-site inspection were likewise very low, corroborating the results observed for the other parameters (Figure 8). To determine representative values of corrosion it will be necessary to monitor the structure, determining corrosion parameters variation with environmental parameters and concrete saturation degree. So these measurements are informing us about the actual corrosion progress but we have no information about what happened before.

In other words, even where the laboratory-measured saturated resistivity values denoted possible corrosion due to low concrete cover resistivity, such problems are unlikely given the absence of chlorides and scant pore water content.

The moisture meter delivered the same readings (30 % to 44 %) for the horizontal and vertical arms of the car park reinforced concrete units. The first and fourth units, the ones closest to the building (Figure 7) that consequently receive less solar radiation, exhibited around 40 % to 43 % moisture content, compared to the 31 % observed in the more distant, less shaded units.

The approximate uniformity of the Schmidt hammer test results at around 52±2 (dimensionless units) for the pergola supports measured was an indication that the surfaces are in good condition. At 60 MPa, the compressive strength extrapolated from the calibration curves furnished by the hammer manufacturer based on the rebound readings was double the value determined on the core samples (Table 2) and 3.5-fold the design specification. According to earlier studies, in most cases extrapolation is unreliable because the rebound measurements vary depending on factors such as surface roughness, moisture content, carbonation, porosity and measuring facility calibration (63, 64).

3.2. Rib-like shell

3.2.1. Historical background and present condition

The reinforced concrete rib-like shell (Figure 9), designed to serve as an outdoor chapel, was built nearly two decades later than the main building, in 1969. Its constructional details are described in Cassinello et al. (37). The 6.5 m high, 10 m long shell is characterised by a complex geometry defined by a Bernoulli lemniscate in which the 40 cm thick base wanes to 6 cm at the outer edge. It is reinforced with steel bars ranging in diameter from 12 mm to 20 mm. When the structure was stripped of the formwork 3 d after casting, the quick set concrete used in its construction exhibited compressive strength of 19 MPa whilst the tip was positioned 12 cm below the design height.

Unlike the pergola, this structure was not initially painted. The form-determined inner surface tex-

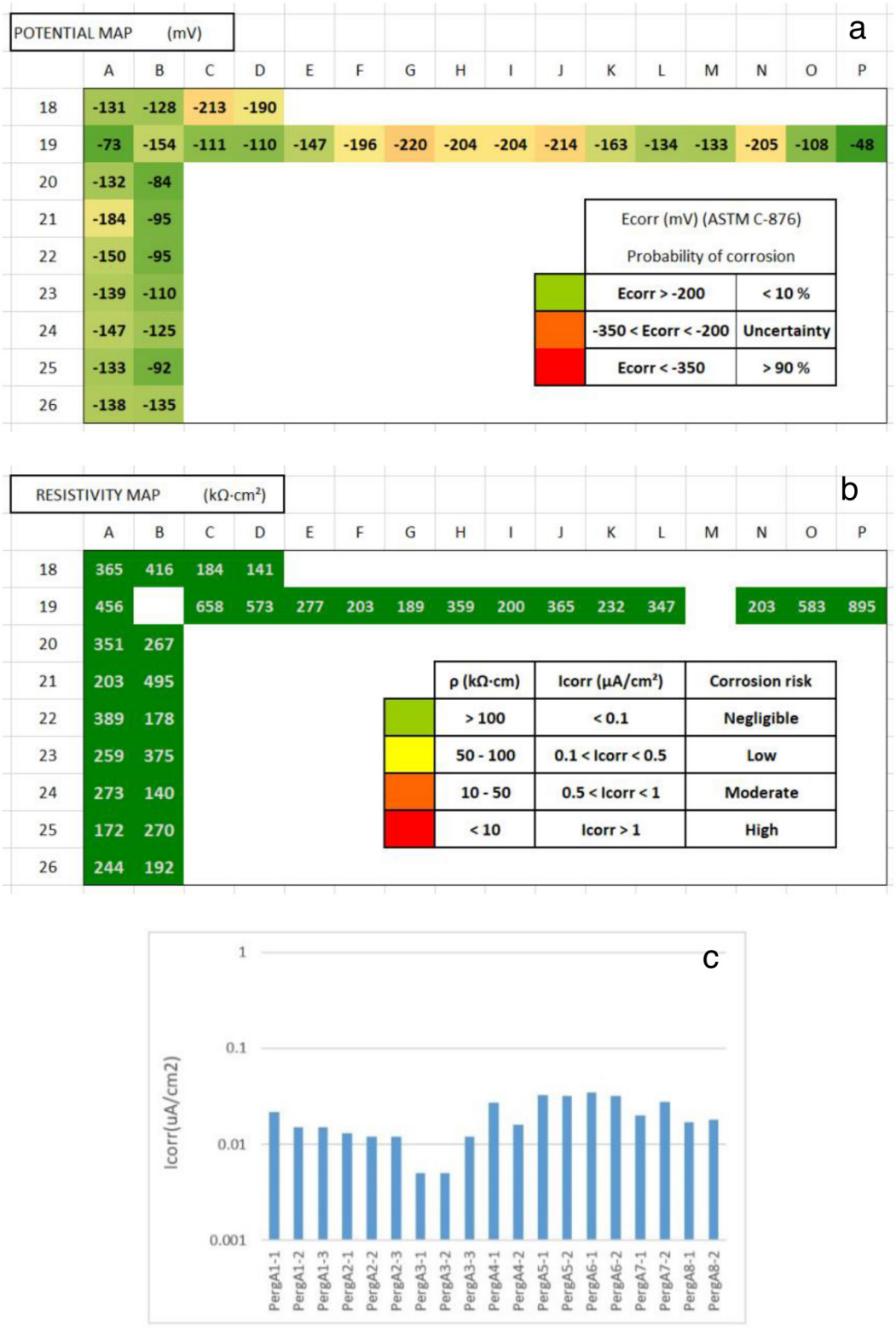

FIGURE 8. In situ corrosion measurements in pergola unit 1: (a) Corrosion potential. (b) Resistivity. (c) Corrosion rate.

ture was not modified, whereas the outer surface was treated with a pneumatic bush-hammer (37). No conservation operations have been undertaken since it was built. In an earlier study Echevarría et al. (50) detected local rusting but no surface cracking, crumbling or weathering nor any other symptom that might denote anomalous structural behaviour.

The damage map drawn on the occasion of this analysis shows corrosion in the areas where the reinforcement is exposed, along with biological colonisation, on the top surface of the shell in particular (Figure 10).

3.2.2. Concrete characterisation

The methodology to determine the key characteristics of the rib-like shell concrete was the same as used for the pergola material.

Two core samples were taken from the rib-like shell, one from the slab and the other from the lower part of the rib (Figure 11), for subsequent mineralogical and physical characterisation. Analysis of the optical micrographs revealed that the mineralogical composition of the gravel differs from design specifications (Table 3), for it comprises not only polycrystalline quartz (with and without muscovite and iron oxides) but biomicrite and sparry calcite. In contrast, the primarily quartz-grain based siliceous composition of the sand, with some K-feldspar and plagioclase, is essentially the same as initially designed. Further to their respective particle size distributions, both aggregates are well-graded, with d/D=2/26.7 in the coarse material and d/D=0.02/4 in

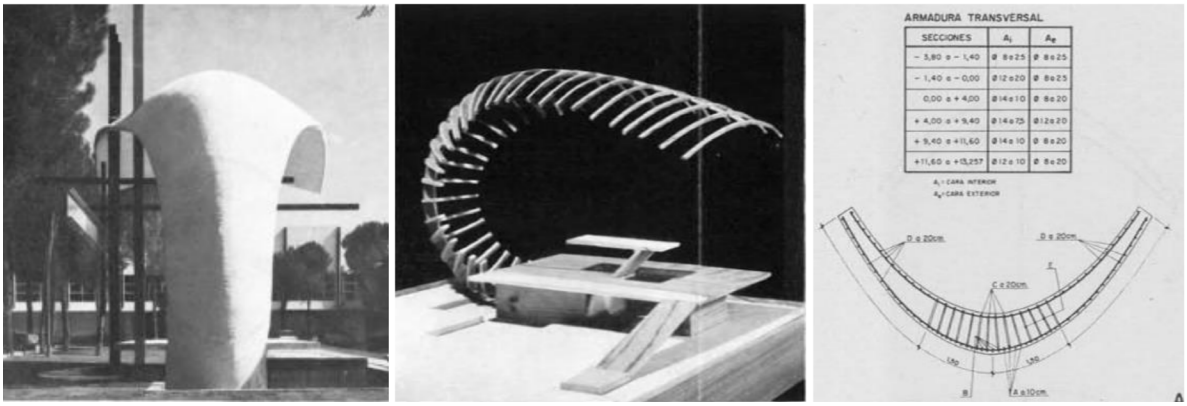

FIGURE 9. Finished shell, reinforcement mock-up and design drawings (37).

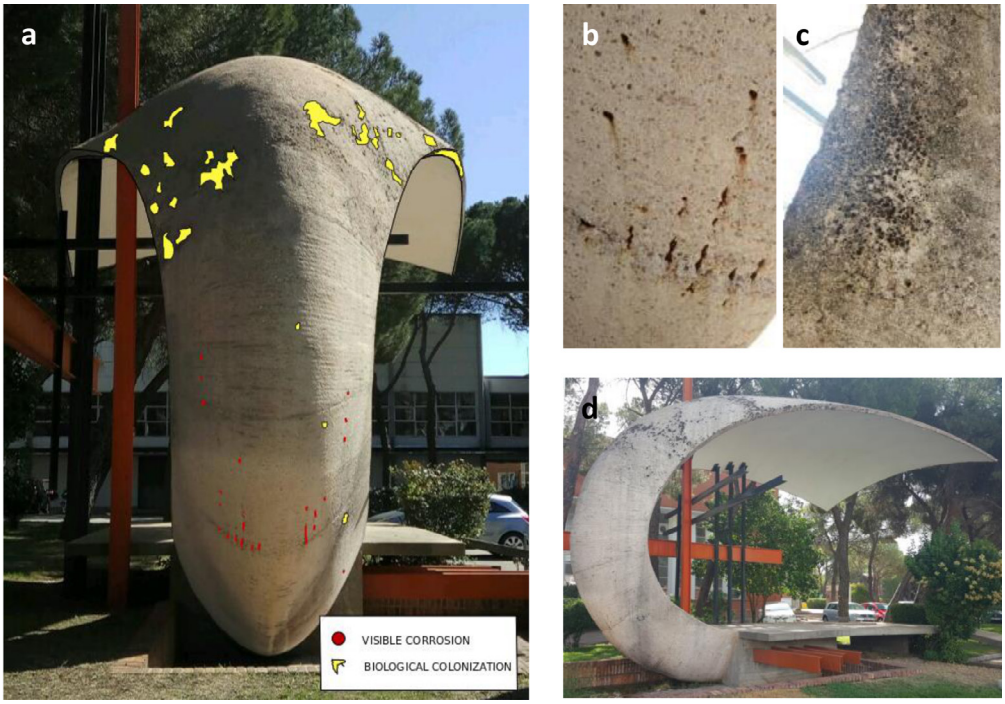

FIGURE 10. Damage in rib-like shell: (a) Diagnosis. (b) Steel corrosion. (c) Biological colonisation. (d) Overview.

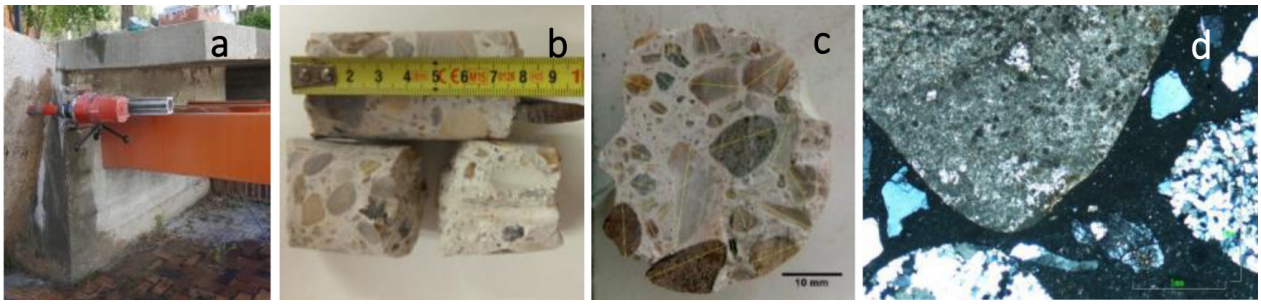

FIGURE 11. (a) Coring the rib-like shell. (b, c) core samples dimensions. (d) SEM micrograph of concrete

the fines.

The most intense reflections observed in the XRD pattern for the high cement paste content fraction were generated by the quartz and calcite aggregates (which had not separated from the paste altogether), although the line attributed to calcite might also be indicative of cement paste carbonation. XRD also detected the presence of gypsum and portlandite, with the latter, according to the DTA-TG findings, accounting for 5.3 wt% and calcite for 20.8 wt% of the total. Those results were corroborated by FT-IR analysis, for the bands characteristic of those minerals were visible on the spectrum.

Compressive strength at 33.3 MPa and Young's modulus at 41.1 GPa were similar to the values expected of healthy concrete and similar as well to the findings observed for the pergola. Corrosion resistance, at dry (447.29 kΩ·cm) and saturated (20.07 kΩ·cm) electrical resistivity values, was higher in the shell than in the pergola and the carbonation front shallower (mean 2.6 mm, maximum 4.1 mm; Figure 12), due largely to its lower porosity (6 %).

3.2.3. In-situ testing

In earlier inspection, Echevarría et al. (50) analysed the structural behaviour of the shell with a 3D laser scan, comparing its present condition to the design specifications. Despite the substantial 373 mm drop at the tip of the overhang, their analysis concluded that the shell complied with existing Spanish legislation on structural safety (65).

Although a cover of up to 40 mm was specified for the slab (Table 3), according to the GPR findings (Figure 13) the concrete protecting the reinforcement from potential environmentally-induced corrosion is <30 mm. In some sporadic instances there is no cover whatsoever (Figure 10), due to the difficulties involved in laying the forms and positioning the reinforcement described by Cassinello et al. (37). Those problems were exacerbated by design specifications calling for a cover of just 10 mm at the unrestrained edge of the structure (Table 3).

The electrical resistivity and corrosion potential

TABLE 3. Key characteristics of rib-like shell concrete.

	Design characteristics (37)	**Findings in this study**	**Eurocode** (56)
Compressive strength (MPa)	19.61 (3 days)	33.3	30
Water-accessible porosity (v/v %)		6	7 – 24
Density (g/cm^3)		2.4	2.4 - 2.9
Type of cement	Rezola white cement	White cement	
Gravel aggregate	Siliceous river gravel	Siliceous and calcareous aggregate	
Sand aggregate	Quartz sand	Quartz sand with potassium feldspar and plagioclase	
Moisture (%)		26.4-39.3	
Ultrasound velocity (m/s)		4363	
MOEus (GPa)		41.1	
Dry resistivity (kΩ·cm)		447.29	
Saturated resistivity (kΩ·cm)		20.97	
Reinforcement bar cover (mm)	Variable from 10 (outer edge) to 40 (base)	<30 (base)	35
Carbonation depth (mm)		2.6 ± 0.8	

findings revealed that the risk of active corrosion in the slab concrete is low at this time (Figure 14), for like in the pergola, the threshold value indicative of steel de-passivation has not been reached.

The dimensionless Schmidt hammer test measurements, at 56±4, denote concrete uniformity, whilst the sole differences in shell moisture content are orientation-dependent, with higher values in the north-facing (39 %) than in the west-facing (26 %) areas.

FIGURE 12. Surface of freshly broken core sample drawn from rib-like shell after spraying with thymolphthalein (blue dye = non-carbonated material)

3.3. Window Frame

3.3.1. Historic background and damage mapping

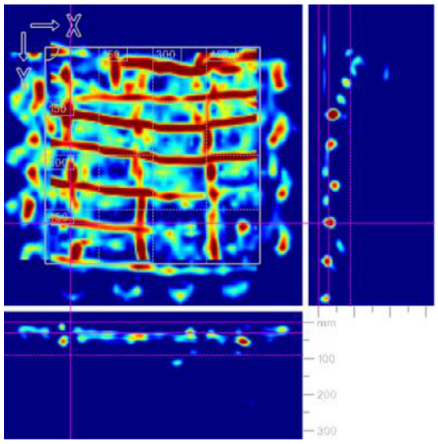

FIGURE 13. Shell reinforcement.

a

POTENTIAL MAP (mV)

	A	B	C	D	E
1	-201	-78	-162	-127	107
2	118	-54	-138	-89	-1
3	39	-26	-158	-72	-98
4	62	7	43	-33	-82
5	150	131		84	-19
6	182	169			

b

RESISTIVITY MAP (kΩ·cm²)

	A	B	C	D	E
1	538	230	155	156	592
2	381	552	112	144	274
3	245	669	502	219	99
4	394	184	432	196	156
5	618	502		306	328
6	878	798			

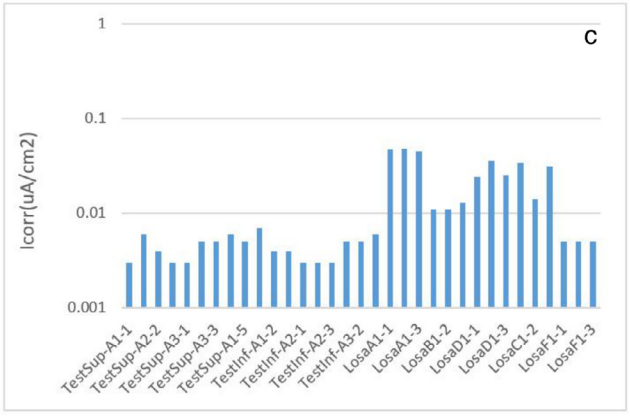

FIGURE 14. In situ corrosion measurement in the rib-like shell slab: (a) Corrosion potential. (b) resistivity. (c) corrosion rate.

The building's 400 low-strength, 1.60 m high window frames were cast at an on-site workshop using mortar with a sand:(white) cement ratio of 1:2. Bearing capacity is provided by the likewise 1.60 m long lintels and the vertical supports (concrete columns). The reinforced concrete columns were cast between the windows into forms comprising the vertical members in the two adjacent window frames as the sides, the indoor building façade at the rear and temporary corrugated sheet steel panel across the front. The latter stripped served as ornamentation in this inter-window space (39) (Figure 15).

The frames have been repainted on a number of occasions predating this analysis.

The present damage map shows both corrosion issues and some cracking. The most prominent problem observed was clogged drainage and the resulting ponding of water in the top member. That in turn has often generated further damage in the form of mortar corrosion and crumbling due to cementitious matrix dissolution. Part of one of the corners on the lintel in poorest condition was observed to have detached completely in response to corrosion (Figure 16).

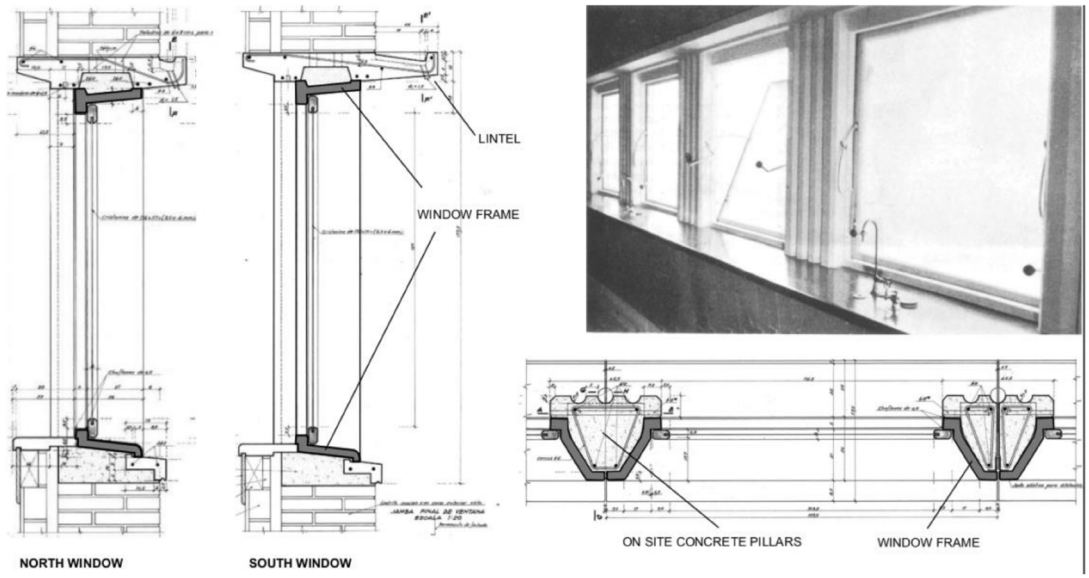

FIGURE 15. Design drawings for window frame assembly and worksite photograph (39).

FIGURE 16. Window damage: (a) Diagnosis. (b) Spalling. (c, d) steel corrosion.

3.3.2. Mortar characterisation

A 29 cm long, 0.87 kg sample was cored from an area in the lintel on one of the windows on the south side of the building where top reinforcement corrosion had induced severe spalling (Table 4).

The petrographic and SEM/EDX (Figure 17) analyses conducted on the sample to characterise the mortar showed that the sand (d/D=0.1/4) comprised well-graded, sub-angular monocrystalline (together with some polycrystalline) quartz grains ranging in size from 100 µm to 4 mm and smaller (250 µm to 3 mm) angular potassium feldspar particles (Table 4). A minor fraction (around 10 %) of 0.5 mm to 1.5 mm plagioclase was also present. Briefly, the design specified the same mineralogy for the mortar sand as for the concrete fines (57).

In addition to the intense quartz and feldspar reflections, the XRD pattern (Figure 18) exhibited signals attributed to mica, hydrated cement phases ettringite and portlandite and cement paste carbonation-induced calcite, all confirmed by FT-IR analysis (Figure 18).

DTA/TG-quantified portlandite content came to 3.7 wt% and calcite content to 10 wt% to 12 wt%. The broad, asymmetrical DTA signal for $CaCO_3$ decarbonation denoted the low crystallinity of that compound.

A comparison of HCl dissolution-based solubility to the TG findings for the sample (46) yielded a cement:sand ratio of 1:1.7, only slightly lower than the design specification.

Despite the well-graded quality of the sand, the mortar is fairly porous, exhibiting mean porosity of 13.7 % (Figure 19), with pores <1 µm accounting for 9 %. Those data, found with mercury intrusion porosimetric techniques, are not comparable to the water-accessible porosity findings described above, however, for the two parameters measure different size pores, the former in the 3 nm to 350 µm range and the latter 50 nm pores only (66).

Nonetheless, at 41.1 GPa the Young's modulus value denotes high mortar quality, although compressive strength could not be determined due to the irregular shape of the sample.

The carbonation depth observed is shallow (mean=1.7 mm), with CO_2 penetration reaching up to 16 mm in only one area, affected by cracking (Table 4).

3.3.3. In-situ testing

The mean thickness of the concrete covering the

TABLE 4. Key characteristics of window frame mortar.

	Design characteristics (39, 57)	**Findings in this study**
Hg intrusion porosity (vol%)		13.7 ± 0.6
Density (g/cm^3)		2.3 ± 0.1
Cement:sand ratio	1:2 (cement:sand)	1:1.7
Type of cement	white cement	white cement
Sand aggregate	Siliceous sand	Siliceous sand (quartz, potassium feldspar and plagioclase)
Moisture (%)		31.7-39.7
Ultrasound pulse velocity (m/s)		4054
Ultrasound-determined longitudinal MOE (MOEus) (GPa)		41.1
Carbonation depth (mm)		1.7 ± 0.6

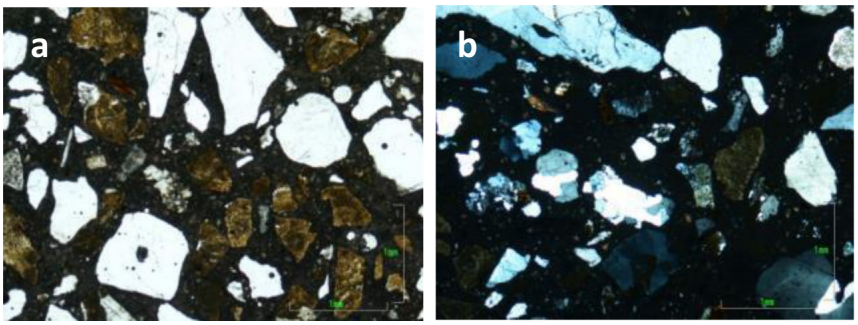

FIGURE 17. Thin section micrographs showing: (a) Sub-angular quartz (white), angular K feldspar (dyed brownish) and plagioclase (grey) particles under plane-polarised light. (b) Primarily mono- and polycrystalline quartz under cross-polarised light.

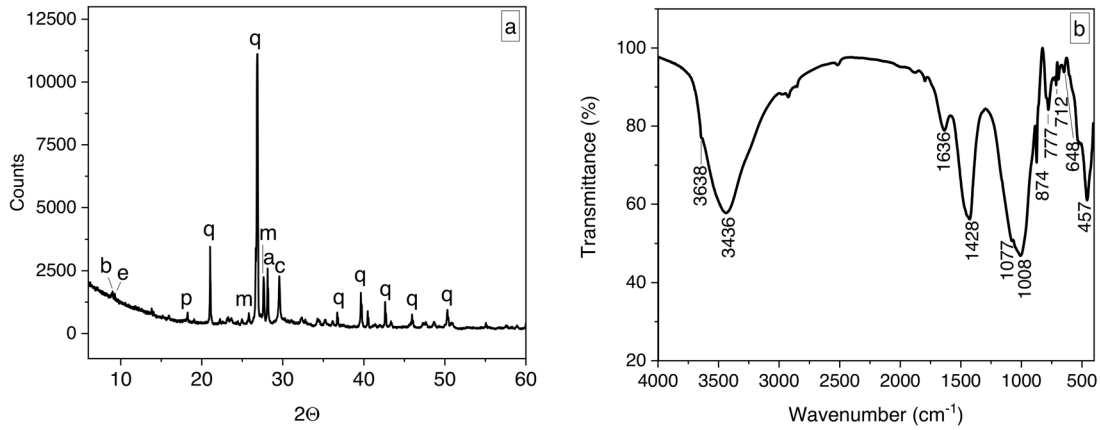

FIGURE 18. (a) XRD pattern for the lintel mortar (b=biotite, COD: 9000025); e=ettringite, COD: 9011103); p=portlandite, COD: 9009098); m=microcline, COD: 9000189); q=quartz, COD: 1011159; a=albite, COD: 9001631); c=calcite, COD: 9007689). (b) FTIR spectrum for the same element.

reinforcement in the precast window frames was also determined. The minimum design thickness was 6 mm (Figure 15), whilst in situ GPR delivered a mean of 15 mm (in the south-facing window the readings were more scattered than in the north, with a maximum thickness of 40 mm and minimum of 0 mm).

Similar moisture content values (32 % to 40 %) were found for the north and south façade vertical framing, whereas content was greater in the south- than in the north-facing lintels. The explanation may lie in the larger size of the south frame lintels, splashed by the rainwater gushing out of the rooftop gargoyles (Figure 16).

The Schmidt hammer rebound values were essentially identical for the north and south frames, with means of 56 and 57, respectively.

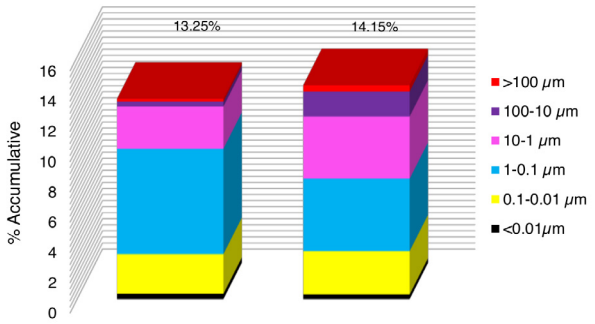

FIGURE 19. Total Hg intrusion porosity and pore size distribution in mortar window frames.

4. CONCLUSIONS

The growing awareness of the cultural significance of 20th century concrete construction works makes imperative an adequate strategy for their preservation for future. Therefore, a strategy based on the continuous monitoring, different from an isolated and purely technical approach, is necessary to first minimize the maintenance required and secondly to propose more respectful interventions. This investigation presents the results of this first characterization and diagnosis phase of three singular concrete or mortars elements at the headquarters of the Eduardo Torroja Institute for Construction in Madrid, Spain. In a following subsection (4.1. Strategy for maintenance) a preliminary protection and prevention proposal is presented for the future application and validation of a selection of novel products developed in the InnovaConcrete project.

The structures, representative of distinct stages in the building construction, were selected for their cultural, historical, aesthetic, social and technological significance in the modern architecture movement within the InnovaConcrete Project.

They were assessed on the grounds of a compilation of the information on building construction, structural analysis of the respective members and characterisation of the constituent materials.

The present condition of the structures, built with essentially no deviation from the initial design are listed below.

General: Judging from Schmidt hammer and ultrasonic velocity measurements, the key structures are all in good condition.

Car park pergola: Even though the core samples proved to be in good condition, the aesthetic value of this element is compromised by the presence of reinforcement-induced cracking around the tips and top surface microcracking attributable to the failure to vibrate the concrete during casting and subsequent biological colonisation. Although with rare presence of exposed reinforcement, in-situ corrosion analyses

denoted low risk of corrosion.

Rib-like shell: The samples cored from the slab of the rib-like shell were likewise in good condition, better in fact than observed in the pergola. Although with presence of exposed reinforcement, no risk of active corrosion was identified in the slab whereas in the shell itself exposed reinforcement is observed. The porosity of the upper surface of the concrete, without any protection, is the cause of subsequent biological colonization.

Window frame: The window frame lintels are not in optimal condition, exhibiting spalling and detachment due to faulty drainage that favour water ponding. The scant coating of the reinforcement has made numerous corrosion points visible.

4.1. Strategy for maintenance

The proposals for intervention to preserve their monumental, artistic and historic values are listed below:

General: Except for the presence of reinforcement-induced cracking around the tips of some pergola in the car park and the cogged drain holes in the window frames, conservation of the elements analysed only requires superficial protection and prevention interventions.

Car park pergola: Cleaning and protection with compatible products are now imperative. Whilst both laboratory and in-situ corrosion analyses denoted low risk of corrosion, application of inhibitors to the exposed steel bars is recommended to prevent surface corrosion. The conservation strategy might be supplemented with the use of micromortars to seal cracks and consolidants to deter material loss. After cleaning, the top of the horizontal elements should be coated with a water repellent to minimise biological colonisation and water access. Cracking around the tips will require the use of repair mortars also compatible with existing materials.

Rib-like shell: No risk of active corrosion was identified in the slab, whereas the presence of exposed reinforcement in some areas suggests that the shell would benefit from the application of corrosion inhibitors and repair mortars. These operations should be supplemented with shell cleaning at the top side, more exposed to rainwater, which should be coated with water repellents to minimise biological colonisation.

Window frame: One possible solution to the problem posed by the small and readily cogged drain holes might consist in enlarging the holes and monitoring the results for some time to determine whether that, in conjunction with periodic cleaning, suffices to ensure effective drainage. After surface cleaning and drainage retooling, material losses should be patch repaired with corrosion inhibitors and water-repellent micromortars. The upper side of the lintels should be treated with water-repellents products to enhance their impermeability.

Given the heritage value of these elements, the techniques and treatments prescribed for their conservation must be verified for chemical and aesthetic compatibility, as well as durability.

ACKNOWLEDGEMENTS

This study was funded by the European Union's Horizon H2020 Research and Innovation Programme under Grant Agreement N$^{o.}$ 760858 (InnovaConcrete) and by the Regional Government of Madrid (TopHeritage-CM; S2018/NMT_4372). The professional support provided by the CSIC's 'Open Heritage: Research and Society (PTI-PAIS)' Interdisciplinary Thematic Platform is gratefully acknowledged.

AUTHOR CONTRIBUTIONS:

Conceptualization: P.M. Carmona-Quiroga, A. Pachón-Montaño, J. Queipo de Llano, I. García-Lodeiro, M.T. Blanco-Varela, E. Frías-López. Formal analysis: P.M. Carmona-Quiroga, A. Pachón-Montaño, J. Queipo de Llano, J.A. Martín-Caro, D. López, I. Paniagua; I. Martínez, F. Rubiano, L. Fernández-Ordóñez, M.T. Blanco-Varela, E. Frías-López. Funding acquisition: M.T. Blanco-Varela. Investigation: P.M. Carmona-Quiroga, A. Pachón-Montaño, J. Queipo de Llano, J.A. Martín-Caro, D. López, I. Paniagua; I. Martínez, F. Rubiano, L. Fernández-Ordóñez, E. Frías-López. Roles/Writing, original draft: P.M. Carmona-Quiroga, A. Pachón-Montaño, J. Queipo de Llano, E. Frías-López. Writing, review & editing: P.M. Carmona-Quiroga, A. Pachón-Montaño, J. Queipo de Llano, I. García-Lodeiro, M.T. Blanco-Varela, E. Frías-López.

REFERENCES

1. Heinemann, H.A.; van Hees, R.P.J.; Nijland, T.G. (2008) Concrete: Too young for conservation? In: D'Ayala & Fodde (Eds), Structural Analysis of Historic Construction (pp. 10). London: Taylor & Francis Group.
2. Ramírez Guerrero, G.; Arcila Garrido, M.; Chica Ruiz, A.; Benítez López, D. (2019). Concrete as heritage: Social perception and its valuing – the Zarzuela hippodrome case. *WIT Trans. Built. Environ.* 191, 17-27. https://doi.org/10.2495/STR190021.
3. Macdonald, S.; Arato Gonçalves, A.P. (2020). Conservation principles for concrete of cultural significance. Los Angeles: Getty Conservation Institute.
4. Damas Mollá, L.; Sagarna Aranburu, M.; Uriarte, J.A.; Aranburu, A.; Zabaleta, A.; García-García, F.; Antigüedad, I.; Morales, T. (2020) Understanding the pioneering techniques in reinforced concrete: the case of Punta Begoña Galleries, Getxo, Spain. *Build. Res. Inf.* 48, 785–801 https://doi.org/10.1080/09613218.2019.1702498.
5. Merzoug, W.; Chergui, S.; Zouaoui, M.C. (2020) The impact of reinforced concrete on the modern-day architectural heritage of Algeria. *J. Build. Eng.* 30, 101210 https://doi.org/10.1016/j.jobe.2020.101210.
6. Jackson, M.D.; Landis, E.N.; Brune, P.F.; Vitti, M.; Chen, H.; Li, Q.; Kunz, M., Wenk, H-R.; Monteiro, P.J.M.; Ingraffea, A.R. (2014) Mechanical resilience and cementitious processes in Imperial Roman architectural mortar. *PNAS.* 111 [5], 18484-18489. https://doi.org/10.1073/pnas.1417456111.
7. Gross, G. (2018) Concrete heritage conservation and the viability of migrating corrosion inhibitors, Master´s Thesis, Columbia University. https://doi.org/10.7916/D8DV32P9.

8. Frampton, K. (2007) Modern architecture: A critical history, London: Thames & Hudson Ltd, 4th edition.
9. Barberena Fernández, A.M. (2016) Conservación de esculturas de hormigón: efecto de consolidantes en pastas y morteros de cemento, Doctoral Thesis, Universidad Complutense de Madrid.
10. Peralbo Cano, R.; Durán Suárez, J.A. (2005) La escultura y la dimensión del hormigón: morteros y hormigones con aplicaciones técnico-escultóricas. Granada: Facultad de Bellas Artes (Departamento de Escultura), Universidad de Granada.
11. Bergeron, L. (2003) L'impact de la modernisation économique et le patrimoine industriel. Word Heritage papers 5, UNESCO.
12. de Almeida Valença, J.M.; Fernandes Pereira de Almeida, C.A.; Miranda Botas, J.L.; Brito Santos Júlio, E.N. (2015) Patch Restoration Method: A new concept for concrete heritage. *Construc. Build. Mat.* 101, 643-651. https://doi.org/10.1016/j.conbuildmat.2015.10.055.
13. Heinemann, H. A. (2013) Historic Concrete. From concrete repair to concrete conservation. Doctoral Thesis, Delft University. https://doi.org/10.4233/uuid:987fafd0-cd76-4230-be0e-be8843cae08e.
14. Berkowski, P.; Dmochowski, G.; Barański, J.; Szołomicki, J. (2018) The construction history and assessment of two heritage industrial buildings in Wrocław. MATEC Web of Conferences, 174, 03008. https://doi.org/10.1051/matecconf/201817403008.
15. Valença, J.; Júlio, E. (2010) Conservation requirements for concrete heritage. The case study of the buildings of the Fundação Calouste Gulbenkian in Lisbon. In: P. J. S. Cruz (Ed.), ICSA 2010, Structures and Architecture, Proceedings of the first international conference on structures and architecture (pp.439-440). Guimares: CRC Press.
16. ACI PRC-201.2-16 (2016) Guide for Durable Concrete. Detroit, American Concrete Institute.
17. Courard, L.; Guillard, A.; Darimont, A.; Bleus, J.M.; Paquet, P. (2012) Pathologies of concrete in Saint-Vincent Neo-Byzantine Church and Pauchot reinforced artificial Stone. *Construc. Build. Mat.* 34, 201-210. https://doi.org/10.1016/j.conbuildmat.2012.02.070.
18. Gaudette, P.; Slaton, D. (2007) Preservation Brief 15 : Preservation of historic concrete. Washington D.C.: National Park Service, Heritage Preservation Services.
19. De Weerdt, K.; Plusquellec, G.; Belda Revert, A.; Geiker, M.R.; Lothenbach, B. (2019). Effect of carbonation on the pore solution of mortar. *Cem. Concr. Res.* 118, 38-56. https://doi.org/10.1016/j.cemconres.2019.02.004.
20. Garcia-Lodeiro, I.; Goracci, G.; Dolado, J.S.; Blanco-Varela, M.T. (2021). Mineralogical and microstructural alterations in a portland cement paste after an accelerated decalcification process. *Cem. Concr. Res.* 140, 106312. https://doi.org/10.1016/j.cemconres.2020.106312
21. Galán, I.; Andrade, C.; Castellote, M. (2012) Thermogravimetrical analysis for monitoring carbonation of cementitious materials. Uptake of CO_2 and deepening in C-S-H knowledge. *J. Therm. Anal. Calorim.* 110 [1], 309-319. https://doi.org/10.1007/s10973-012-2466-4.
22. Di Mundo, R.; Labianca, C.; Carbone, G.; Notarnicola, M. (2020). Recent advances in hydrophobic and icephobic surface treatments of concrete. *Coatings.* 10 [5], 449. https://doi.org/10.3390/coatings10050449.
23. BS EN 1504-9:2011. Products and systems for the protection and repair of concrete structures - Definitions, requirements, quality control and evaluation of conformity - Part 9: General principles for the use of products and systems. London: BSI.
24. Pizzigatti, C.; Franzoni, E. (2021) The problem of conservation of XX century architectural heritage: The fibreglass dome of the woodpecker dance club in Milano Marittima (Italy). *J. Build. Eng.* 42, 102476 https://doi.org/10.1016/j.jobe.2021.102476.
25. Arato Gonçalves, A.P.; Macdonald, S.; Marie-Victoire, E.; Bouichou, M.; Wood, C. (2019). Performance of patch repairs on historic concrete structures: a preliminary assessment. MATEC Web of Conferences, 289, 0700. https://doi.org/10.1051/matecconf/201928907001.
26. Borg, R.P. (2020) Concrete heritage: challenges in conservation. Symposia Melitensia, 16, 35-52.
27. Kapetanaki, K.; Vazgiouraki, E.; Stefanakis, D.; Fotiou, A.; Anyfantis, G.C.; García-Lodeiro, I.; Blanco-Varela, M.T.; Arabatzis, I.; Maravelaki, P.N. (2020) TEOS modified with nano-calcium oxalate and PDMS to protect concrete based cultural heritage buildings. *Front. Mater.* 7, 1-13. https://doi.org/10.3389/fmats.2020.00016.
28. Courard, L.; Zhao, Z.; Michel, F. (2021) Influence of hydrophobic product nature and concentration on carbonation resistance of cultural heritage concrete buildings. *Cem. Concr. Comp.* 115, 103860. https://doi.org/10.1016/j.cemconcomp.2020.103860.
29. InnovaConcrete project (2018-2021) Retrieved from https://www.innovaconcrete.eu.
30. DOCOMOMO Iberico, ICOMOS (2019) 100 from the 20th, the InnovaConcrete selection of the significant 20th Century heritage sites in Europe. Retrieved from https://www.innovaconcrete.eu/100-from-the-20th-is-online-now/.
31. Queipo-de-Llano, J.; Pachón-Montaño, A.; García-Lodeiro, I.; Carmona-Quiroga, P.M.; Blanco-Varela, M.T.; Frías-López, E. (2018) Singular elements in the architecture of the IETCC: design, execution and current status. In: Cassinello (Ed.), International Conference on Construction Research - EDUARDO TORROJA. Architecture, Engineering, Concrete. Madrid.
32. DOCOMOMO Ibérico. Documentation and conservation of the architecture and urbanism of the modern movement. Retrieved from http://www.docomomoiberico.com.
33. Equipo Editorial. (1984) Conmemoración del cincuenta aniversario del Instituto de la Construcción y del Cemento «Eduardo Torroja». *Inform. Construc.* 36 [365], 5–22. https://doi.org/10.3989/ic.1984.v36.i365.1893.
34. Azorín, V.; Cassinello, P.; Monjo, J. (2012) Archivo Eduardo Torroja. La Sede del itcc (1949-1953). Inéditos anteproyectos previos a su construcción. *Infor. Constr.* 64 [525], 5–18. https://doi.org/10.3989/ic.11.023.
35. Equipo Editorial. (1958) Costillares. Instituto Técnico de la Construcción y del Cemento. *Infor. Constr.* 10 [099], 7–26. https://doi.org/10.3989/ic.1958.v10.i099.5575.
36. Echegaray, G.; Barbero, M. (1999) Composición arquitectónica. *Infor. Constr.* 51 [462], 19–42. https://doi.org/10.3989/ic.1999.v51.i462.857.
37. Cassinello, F.; Torroja, J.A.; Morán, F.; Fernández, F. (1969) Morfogénesis de una lámina, España. *Infor. Constr.* 22 [214], 3-28. https://doi.org/10.3989/ic.1969.v22.i214.3659.
38. Nadal, J. (1999) El Instituto Técnico de la Construcción y del Cemento. *Infor. Constr.* 51 [462], 9–18. https://doi.org/10.3989/ic.1999.v51.i462.
39. Eymar, J.M. (1999) Prefabricación. *Infor. Constr.* 51[462], 43–62. https://doi.org/10.3989/ic.1999.v51.i462.858.
40. Archivo Histórico del Instituto Eduardo Torroja-CSIC. Retrieved from https://www.ietcc.csic.es/wp-content/uploads/2017/02/Archivo_Historico.pdf.
41. AEMET, Agencia Estatal de Meteorología, Spain. Retrieved from http://www.aemet.es/es/serviciosclimaticos/datosclimatologicos/valoresclimatologicos?l=3195&k=28.
42. Ayuntamiento de Madrid, Subdirección General de Energía y Cambio Climático (2016) Inventario de emisiones de gases de efecto invernadero del municipio de Madrid. Retrieved from http://www.mambiente.madrid.es/opencms/export/sites/default/calaire/Anexos/InventarioGEI2016.pdf.
43. Ayuntamiento de Madrid, Dirección General de Sostenibilidad y Control Ambiental (2019) Retrieved from https://transparencia.madrid.es/UnidadesDescentralizadas/Sostenibilidad/CalidadAire/Publicaciones/Memorias_anuales/Ficheros/Memoria_2019.pdf.
44. BS EN 12620:2003+A1:2009. Aggregates for concrete. London: BSI.
45. BS EN 14630:2007. Products and systems for the protection and repair of concrete structures - Test methods - Determination of carbonation depth in hardened concrete by the phenolphthalein method. London: BSI.
46. ASTM C1084-19 (2019) Standard Test Method for Portland-Cement Content of Hardened Hydraulic-Cement Concrete. West Conshohocken: ASTM International.
47. UNE 83980:2014. Durabilidad del hormigón. Métodos de ensayo. Determinación de la absorción de agua, la densidad

y la porosidad accesible al agua del hormigón. Madrid: AENOR.
48. BS EN 12390-3:2020. Testing hardened concrete - Part 3: Compressive strength of test specimens. London: BSI.
49. UNE 83988-1:2008. Determinación de la resistividad eléctrica. Parte 1: Método directo (método de referencia). Madrid: AENOR.
50. Echevarría, L.; Garnica, C.; Gutiérrez, J. (2014) La costilla laminar del Instituto de Ciencias de la Construcción Eduardo Torroja (IETcc-CSIC). Levantamiento mediante láser-escáner y evaluación estructural. *Infor. Constr.* 66 [536], e038. https://doi.org/10.3989/ic.14.116.
51. BS EN 12504-2:2013. Testing concrete in structures - Part 2: Non-destructive testing - Determination of rebound number. London: BSI.
52. ASTM C876-15 (2015) Standard test method for corrosion potentials of uncoated reinforcing steel in Concrete. West Conshohocken: ASTM International.
53. Polder, R.; Andrade, C.; Elsener, B.; Vennesland, Ø.; Gulikers, J.; Weidert, R.; Raupach, M. (2000) Test methods for on site measurement of resistivity of concrete. *Mater. Struct.* 33*,* 603–611. https://doi.org/10.1007/BF02480599.
54. Andrade, C.; Martinez, I. (2005) Calibration by gravimetric losses of electrochemical corrosion rate measurement using modulated confinement of the current. *Mater. Struct.* 38*,* 833-841. https://doi.org/10.1007/BF02481656.
55. Polder, R.B. (2001) Test methods for on site measurement of resistivity of concrete - a RILEM TC-154 technical recommendation. *Construc. Build. Mat.* 15*,* 125-131. https://doi.org/10.1016/S0950-0618(00)00061-1.
56. BS EN 1992-1-1:2013/A1:2015. Eurocode 2 Design of concrete structures. Part 1-1 General rules and rules for buildings. London: BSI.
57. Centro Experimental de Arquitectura (1948) Pliego general de condiciones varias de la edificación. Título 1, Condiciones generales de índole técnica; aprobado por el Consejo Superior de los Colegios de Arquitectos; adoptado en las Obras de la Dirección General de Arquitectura. Madrid.
58. Peña Boeuf, A. (1944) ORDEN de 20 de marzo de1944 por la que se aprueba la Instrucción definitiva para el proyecto de ejecución de obras de hormigón. Boletín Oficial del Estado, nº. 153, 4299-4318.
59. Martínez-Ramírez, S.; Zamarad, A.; Thompson, G.E.; Moore, B. (2002) Organic and inorganic concrete under SO_2 pollutant exposure. *Build. Environ.* 37, 933–937. https://doi.org/10.1016/S0360-1323(01)00065-8.
60. Bautista, A.; Velasco, F.; Torres-Carrasco, M. (2019) Influence of the alkaline reserve of chloride-contaminated mortars on the 6-year corrosion behavior of corrugated UNS S32304 and S32001 stainless steels. *Metals.* 9, 686. https://doi.org/10.3390/met9060686.
61. Gadsden, J. A. (1975) Infrared spectra of minerals and related inorganic compounds. London: Butterworth Groups.
62. Ministerio de Fomento (2019) Documento Básico de Seguridad Estructural, DB-SE. Real Decreto 732/2019, de 20 de diciembre, por el que se modifica el Código Técnico de la Edificación. Boletín Oficial del Estado, 311, 140488-140674.
63. Sanchez, K.; Tarranza, N. (2014) Reliability of rebound hammer test in concrete compressive strength estimation. *Int. J. Adv. Agric. Environ. Eng.* 1*,* 198-202. Retrieved from https://iicbe.org/upload/2458C1114040.pdf.
64. Malhotra V.M.; Carino, N.J. (2004) Handbook on nondestructive testing of concrete. Boca Raton: CRC Press.
65. Presidencia del Gobierno (2008) Real Decreto 1247/2008, de 18 de julio, por el que se aprueba la instrucción de hormigón estructural (EHE-08). Boletín Oficial del Estado, nº 203, 35176-35178 y Suplemento.
66. Kéri, A.; Sápi, A.; Ungor, D.; Sebok, D.; Csapó, E.; Kónya, Z.; Galbács, G. (2020) Porosity determination of nano- and sub-micron particles by single particle inductively coupled plasma mass spectrometry. *J. Anal. Atomic Spectrom.* 35*,* 1139-1147. https://doi.org/10.1039/D0JA00020E.